Sensors & Diagnostics

COMMUNICATION

View Article Online
View Journal | View Issue

Check for updates

Cite this: *Sens. Diagn.*, 2024, **3**, 817

Received 4th January 2024,
Accepted 16th April 2024

DOI: 10.1039/d4sd00004h

rsc.li/sensors

Open Access Article. Published on 17 April 2024. Downloaded on 2/17/2026 1:49:50 PM.
This article is licensed under a Creative Commons Attribution 3.0 Unported Licence.

Flexible dual-action colorimetric-electronic amine sensors based on *N*-annulated perylene diimide dyes†

Michael J. Grant, [a] Anderson Hoff,[a] Loren G. Kaake[b] and Gregory C. Welch *[a]

We report the synthesis and characterization of two new molecules based on the *N*-annulated perylene diimide (PDIN-H) dye, modified with an octyl sulfide or octyl sulfone group. The octyl sulfone group increases electron affinity of the PDI core for higher sensitivity to amine detection in both solution and film, which was validated by using a flexible electronic sensing platform towards *n*-butylamine detection.

Food security, safety, and waste are three very different, but closely related problems facing the modern world. Food insecurity and waste are growing global issues.[1–4] Clearly, increasing the efficiency of food systems presents a means to address both the problems. A contributor to the problem of food waste is the use of unreliable and inconsistent date labelling systems. Replacing date labels with a sensor-based system is appealing to reduce the quantity of safe-to-eat food which is discarded. One approach for creating food safety sensors is through the use of biogenic amine sensors. Biogenic amines are released by spoiling foods, particularly protein-rich foods, primarily through a decarboxylation of amino acids. The volatility and basicity of these biogenic amines make them promising for detection by gas sensors. This direct detection of food spoilage byproducts provides an obvious solution to the problems surrounding food safety and food waste.

Many previous systems have been reported for light-based or electronic amine sensing.[5–15] Among these, a number of different sensing mechanisms have been explored to induce an electronic or colour response, including: acid–base chemistry, complexation, charge transfer and many others. A wide variety of materials have also been applied for the purpose of amine sensing, including metal oxides,[9–11] carbon nanomaterials,[12,13] biomaterials[14,15] and organic materials.[5–8] Among the organic small molecules, a widely explored class of molecules for amine sensing are perylene diimides (PDIs). Sensors have been fabricated based on PDI and related systems taking advantage of intermolecular charge transfer,[16–18] aminolysis,[19] radical formation,[20] and others.[21,22]

Previously, we have demonstrated the use of reverse acid-dying for processing films of *N*-annulated perylene diimide (PDIN-H).[23] We noticed that amine bases were capable of inducing an obvious colour change in solution through an acid–base mechanism. PDIs and PDIN-H derivatives are also very well established as semiconductors which can be incorporated into organic electronics.[21,24,25] PDIN-H sensors would be capable of both colorimetric sensing, through the deprotonation of the pyrrolic N–H, and electronic sensing through ion charge transfer through the PDI core as demonstrated by Kaake and co-workers with a PDIN-H based amine sensor through combination with P(NDI2OD-2T).[26] These sensors enabled very high sensitivity, though the inclusion of a coloured conductive polymer does not allow for colorimetric sensing.

A system was designed to study the effects of perimeter modification of the PDIN-H core on the acidity and thus

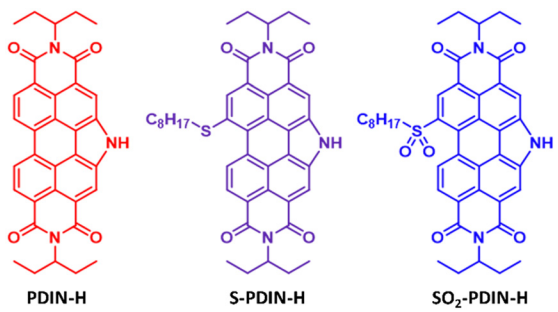

Fig. 1 Structure of PDIN-H and derivatives S-PDIN-H and SO_2-PDIN-H.

[a] *Department of Chemistry, University of Calgary, 2500 University Drive N.W, Calgary, Alberta, T2N 1N4, Canada. E-mail: gregory.welch@ucalgary.ca*
[b] *Department of Chemistry, Simon Fraser University, Vancouver, British Columbia, V5A 1S6, Canada*

† Electronic supplementary information (ESI) available: Experimental and synthetic details. Details on sensor fabrication and testing, optical absorption, cyclic voltammetry, photoluminescence spectroscopy. See DOI: https://doi.org/10.1039/d4sd00004h

© 2024 The Author(s). Published by the Royal Society of Chemistry

Open Access Article. Published on 17 April 2024. Downloaded on 2/17/2026 1:49:50 PM.
This article is licensed under a Creative Commons Attribution 3.0 Unported Licence.

function as a sensor for amine gases. Previously, a number of perimeter modifications have been studied in our lab,[27,28] but none enabled a direct comparison of electron donating and withdrawing groups. For this reason, we selected modification with a sulfide group (Fig. 1). In particular, we selected an alkyl sulfide due to the additional solubility it could provide thus increasing solution processing options. Further, we sought to employ these core modified PDIN-H molecules in a dual-action colorimetric electronic sensor using a transparent conductor, SnO_2.

Materials synthesis is detailed in Fig. S1.† The target molecules feature a core of PDIN-H modified with an octyl sulfide (S-PDIN-H) or an octyl sulfone (SO_2-PDIN-H). PDIN-H derivatives are produced by first SR for Br substitution to yield S-PDIN-H (88% yield) followed by subsequent oxidation with excess *meta*-chloroperoxybenzoic acid to yield the SO_2-PDIN-H (67% yield).

NMR spectra of PDIN-H, S-PDIN-H and SO_2-PDIN-H (Fig. 2) reflect the hypothesized effect from donating and withdrawing groups, respectively. This effect is most visible through tracking the pyrrolic N–H signal (*ca.* 12.03 ppm for PDIN-H). S-PDIN-H shows an upfield shift (*ca.* 11.52 ppm) relative to PDIN-H, indicating increased electron density and reduced acidity. Inversely, SO_2-PDIN-H shows a downfield shift (*ca.* 12.44 ppm) indicative of reduced electron density and increased acidity.

The electrochemical properties of S-PDIN-H and SO_2-PDIN-H were determined by cyclic voltammetry and show similar results to the NMR spectroscopic studies (Fig. 2). S-PDIN-H shows two reversible reduction waves at −1.28 and −1.50 V and one reversible oxidation wave at 0.90 V. SO_2-PDIN-H shows two reversible waves at −1.04 and −1.35 V with an oxidation wave visible at 1.24 V *vs.* the ferrocene-ferrocenium redox couple. Relative to PDIN-H, this demonstrates the expected results. The donating effect of the sulfide group makes the core more electron rich and thus lowers the oxidation potential of the core. Similarly, the withdrawing effect of the sulfone group makes the core more electron poor and thus lowers the reduction potential and increases the oxidation potential. Additionally, UV-visible (UV-vis) spectroscopy was performed in solutions of 2-methyltetrahydrofuran (2-MeTHF, Fig. 2). Both S-PDIN-H and SO_2-PDIN-H are bathochromically shifted relative to PDIN-H (λ_{max} = 519 nm), with maxima at 538 nm and 535 nm, consistent with the energy gap reduction observed in cyclic voltammetry.

UV-vis spectroscopy was used to characterize the deprotonation process in both solutions and solid-state films. Solutions of PDIN-H, S-PDIN-H or SO_2-PDIN-H were studied in DMSO with and without 1,8-biazabicyclo[5.4.0]undecane (DBU, Fig. 3). Upon the introduction of base and consequently deprotonation of the PDI, a large bathochromic shift is observed. Subsequent addition of trifluoroacetic acid to deprotonated solutions reversed this shift to the original profile (Fig. S12†) demonstrating the reversibility of this process.

PDIN-H, S-PDIN-H and SO_2-PDIN-H solutions were then exposed to different concentrations of *n*-butylamine to test the compounds utility as amine sensors. In solution, SO_2-PDIN-H was found to be the most sensitive towards amines, with a noticeable response at 4 ppm butylamine (Fig. 4). S-PDIN-H and PDIN-H were found to begin responding at 12 ppm and 10 ppm, respectively. Curiously, the absorbance ratio of S-PDIN-H increases more rapidly than for PDIN-H despite its response starting later. SO_2-PDIN-H also showed a much stronger response than S-PDIN-H and PDIN-H for example, at 15 ppm butylamine, the absorbance ratio of SO_2-PDIN-H is 16 times greater than for than for PDIN-H.

Further, UV-vis spectroscopy was used to measure the solubility of each compound in the solvent used for processing sensors, 2-MeTHF. PDIN-H was determined to be soluble in 2-MeTHF up to 5 mg mL^{-1} (9 mM, Fig. S14†). S-PDIN-H shows a 7-fold increase in solubility up to 35 mg mL^{-1} (51 mM) and SO_2-PDIN-H shows a 40-fold increase in solubility, up to 208 mg mL^{-1} (289 mM).

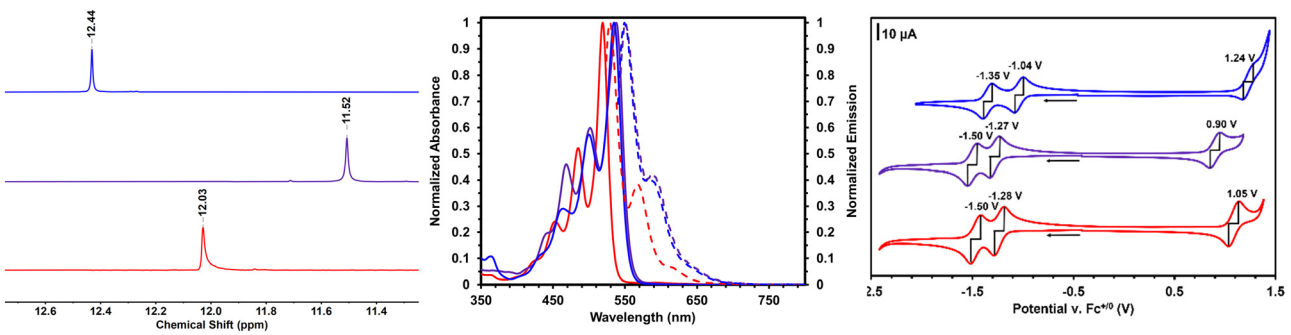

Fig. 2 NMR spectra, UV-visible absorbance, and emission spectra and cyclic voltammograms for PDIN-H (red) S-PDIN-H (purple) and SO_2-PDIN-H (blue). Left: NMR spectra highlighting the N–H proton showing a 0.41 ppm shift downfield for SO_2-PDIN-H and a 0.49 ppm shift upfield for S-PDIN-H relative to PDIN-H. Centre: Absorbance and emission spectra of PDIN-H, S-PDIN-H and SO_2-PDIN-H in 2-methyl tetrahydrofuran solution. Solid lines show absorbance spectra and dashed lines show emission spectra. Right: Cyclic voltammograms showing the resulting decrease in oxidation potential for S-PDIN-H and the decrease in reduction potential and increase in oxidation potential for SO_2-PDIN-H relative to PDIN-H.

© 2024 The Author(s). Published by the Royal Society of Chemistry

Open Access Article. Published on 17 April 2024. Downloaded on 2/17/2026 1:49:50 PM.
This article is licensed under a Creative Commons Attribution 3.0 Unported Licence.

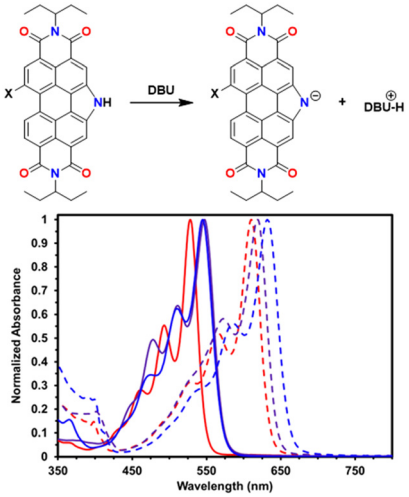

Fig. 3 Top: Deprotonation of PDIN-H derivatives with DBU. Bottom: UV-visible spectra of PDIN-H (red), S-PDIN-H (purple) and SO_2-PDIN-H (blue) in DMSO solution. Solid lines show neat spectra and dashed lines show solutions in the presence of excess DBU.

Films of PDIN-H, S-PDIN-H and SO_2-PDIN-H were slot-die coated onto PET (see ESI†) and compared to additional films printed from a blend with DBU to characterize the solid-state spectrum of each anion. Neat films for each derivative show a broad absorbance centred at approximately 530 nm (Fig. 5). The DBU blended films show a similar trend to that observed in solution, with a large bathochromic shift relative to the neat films. In addition, the spectra of neat films of each PDIN-H were then measured on exposure to *n*-butylamine vapor, and these deprotonated films show a clear difference relative to those blended with DBU (Fig. S15†). This is indicative of a difference in the aggregation of films coated with and without DBU, although it is not clear whether this effect arises from coating in the anionic form or from the presence of DBU acting as a high-boiling solvent and allowing further organization. Over time, a clear change is observed at differing rates. SO_2-PDIN-H shows a rapid conversion, with its spectrum stabilizing within 30 seconds

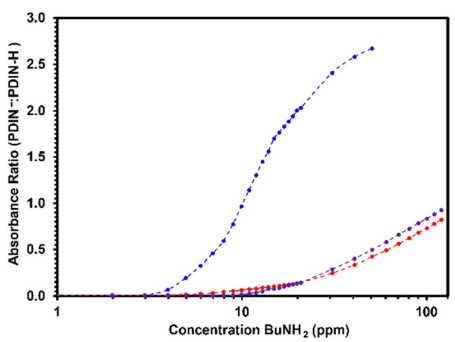

Fig. 4 Colorimetric response of solution phase sensing of $BuNH_2$ for PDIN-H (red), S-PDIN-H (purple) and SO_2-PDIN-H (blue). Absorbance ratio is calculated as the absorbance at the λ_{max} for the PDIN$^-$ species divided by the absorbance at λ_{max} for the PDIN-H species.

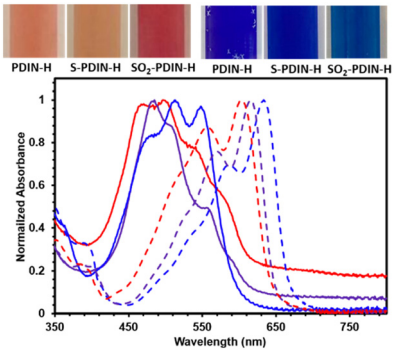

Fig. 5 Top: Images of neat (left) and DBU blended films (right). Bottom: UV-visible spectra of films of PDIN-H (red), S-PDIN-H (purple) and SO_2-PDIN-H (blue) processed from 2-MeTHF (S-PDIN-H and SO_2-PDIN-H) or $BuNH_2$ (PDIN-H) *via* slot-die coating without (solid lines) and with DBU based added (dashed lines).

of injecting *n*-butylamine. S-PDIN-H and PDIN-H convert much more slowly, with conversion stabilizing within 120 seconds and 150 seconds, respectively. This time-response trend is consistent with the sensitivity observed in solution, and thus it is inferred that the film sensitivity follows a similar trend. The observed colour change rapidly reversed once removed from *n*-butylamine exposure.

Electronic sensors were fabricated by slot-die coating a bilayer structure with SnO_2 nanoparticles and the PDIN-H films upon prefabricated interdigitated silver electrodes (IDE) to quantify the electronic changes induced by the deprotonation process. Details of the fabrication process and images of the printed sensors are in experimental procedures section and Fig. S19 in the ESI,† respectively. The SnO_2 NPs is a transparent film allowing for visual detection of colour change, and it can be easily printed from solution on top of the IDE platform PET/Ag. In addition, the SnO_2 NPs is a n-type oxide that can benefit from charge transfer from the PDIN-H upon deprotonation, with consequently increase in its film conductivity. Then, upon exposure of these sensors to *n*-butylamine, a response is measured as the increase in conductance in the SnO_2/PDIN-H film. To investigate the sensing response of the PDIN-H derivative films towards amine, the concentration of *n*-butylamine was systematically

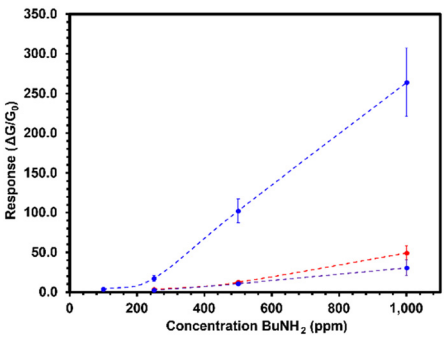

Fig. 6 Response of PDIN-H (red), S-PDIN-H (purple) and SO_2-PDIN-H (blue) electronic sensors to different concentrations of *n*-butylamine vapor.

Open Access Article. Published on 17 April 2024. Downloaded on 2/17/2026 1:49:50 PM. This article is licensed under a Creative Commons Attribution 3.0 Unported Licence.

varied from 100 ppm to 1000 ppm and changes in the current intensity (and consequently the conductance between the two terminals) observed. The corresponding response ratio for the three PDI films, PDIN-H, S-PDIN-H and SO_2-PDIN-H was then plotted as a function of *n*-butylamine concentration, as shown in Fig. 6. The results are averaged from measurements on three independent sensors for each structure, and error bars represent the standard deviation. Sensors with SO_2-PDIN-H show a response of 3.7 at 100 ppm. However, due to equipment limitation, it was not possible to detect the response of PDIN-H or S-PDIN-H under 100 ppm, or for concentrations lower than 100 ppm. The sensors with PDIN-H, S-PDIN-H and SO_2-PDIN-H show the respective response of 3.4, 2.5 and 17 under 250 ppm, 12.3, 10.6 and 102.2 under 500 ppm, and 49.0, 30.2 and 264.1 under 1000 ppm *n*-butylamine. The results are summarized in Table S1.† As can be seen, the response of PDIN-H is slightly higher than that of S-PDIN-H. Also, notably, the response of SO_2-PDIN-H is about one order of magnitude higher than PDIN-H or S-PDIN-H. These results are in agreement with the previous analysis in solution and our initial premise that the octyl sulfone makes the PDI core more electron deficient and consequently more reactive to electron-rich compounds such as amines. Regarding the film colour change, it was not observed at a naked eye for SO_2-PDIN-H under 1000 ppm, and it only became distinguishable under >5000 ppm of *n*-butylamine, saturating under more than 20 000 ppm (Fig. S21†).

Moreover, we tested devices with neat SnO_2 nanoparticles film, to further compare its performance with that of SO_2-PDIN-H, as metal oxides are known to be sensitive to many gas-phase analytes and have been thus applied to many sensing applications.[9,29,30] On exposure to 1000 ppm of *n*-butylamine, SO_2-PDIN-H sensors show a near 3-fold increase in response over neat SnO_2, with a response ratio of 264, compared to 108 for SnO_2. Although neat SnO_2 show high response to *n*-butylamine, we observed that SO_2-PDIN-H sensors show much higher selectivity towards amines than neat SnO_2, as devices with only the SnO_2 film, and SnO_2/SO_2-PDINH were tested upon exposure to pentane, ethanol (EtOH), acetone, ethyl acetate (EtOAc), and water. Both sensing structures did not respond to pentane or acetone. On the other hand, SnO_2 films responded to EtOAc and EtOH (response ratio of 2 and 100, respectively), whereas the SO_2-PDIN-H film did not show any variation in its conductance under exposure to the respective analytes (see ESI†). We also observed a high contrast response ratio to water, of more than 2000 when a device with neat SnO_2 film is exposed to a 50% relative humidity level, whereas device with SnO_2/SO_2-PDINH have a response of 122. It may be noted that the high sensitivity of SnO_2 to water places a challenge for real world applications of the SnO_2/PDIN-H sensing structure, as SnO_2 has application as a humidity sensor.[30–32] In future works, we aim to replace it with more suitable n-type semiconductors, such as polymers with hydrophobic properties in order to keep its conductivity unaffected when performing measurements under high humidity levels.

In summary, we synthesized two new PDIN-H molecules, S-PDIN-H and SO_2-PDIN-H, with higher solubility in green solvents and superior amine detection capability. A dual colour and electronic response were quantified, with a sensing response to *n*-butylamine one order of magnitude higher for SO_2-PDIN-H sensors compared to PDIN-H and S-PDIN-H. The improved performance of SO_2-PDIN-H was attributed to its higher electron affinity and consequently higher reactivity to electron-rich compounds, and this approach could be applied to the design of efficient molecules for detection of other targets beyond amines.

Conflicts of interest

There are no conflicts to declare.

Notes and references

1 Access to food in 2020. Results of twenty national surveys using the Food Insecurity Experience Scale (FIES), FAO, 2021.
2 The State of Food Security and Nutrition in the World 2021, FAO, IFAD, UNICEF, WFP and WHO, 2021.
3 D. Gunders, *Wasted: How America Is Losing Up to 40 Percent of Its Food from Farm to Fork to Landfill*, 2017.
4 J. Gustavsson, C. Cederberg, U. Sonesson, R. van Otterdijk and A. Meybeck, *Global Food Losses and Food Waste: Extent, Causes and Prevention*, Food and Agriculture Organization of the United Nations, Rome, 2011.
5 M. J. Grant, K. M. Wolfe, C. R. Harding and G. C. Welch, *J. Mater. Chem. C*, 2023, **11**, 9749–9767.
6 R. S. Andre, L. A. Mercante, M. H. M. Facure, R. C. Sanfelice, L. Fugikawa-Santos, T. M. Swager and D. S. Correa, *ACS Sens.*, 2022, **7**, 2104–2131.
7 D. Gomes Müller, E. Quadro Oreste, M. Grazielle Heinemann, D. Dias and F. Kessler, *Eur. Polym. J.*, 2022, **175**, 111221.
8 S. K. Kannan, B. Ambrose, S. Sudalaimani, M. Pandiaraj, K. Giribabu and M. Kathiresan, *Anal. Methods*, 2020, **12**, 3438–3453.
9 Y. Xu, L. Zheng, C. Yang, W. Zheng, X. Liu and J. Zhang, *ACS Appl. Mater. Interfaces*, 2020, **12**, 20704–20713.
10 S. Büyükköse, *Mater. Sci. Semicond. Process.*, 2020, **110**, 104969.
11 V. Solanki, A. Banerjee and K. K. Nanda, *Sens. Actuators, B*, 2022, **366**, 131942.
12 R. Ghosh, A. Singh, S. Santra, S. K. Ray, A. Chandra and P. K. Guha, *Sens. Actuators, B*, 2014, **205**, 67–73.
13 J.-W. Han, B. Kim, J. Li and M. Meyyappan, *RSC Adv.*, 2013, **4**, 549–553.
14 H. Vasconcelos, L. C. C. Coelho, A. Matias, C. Saraiva, P. A. S. Jorge and J. M. M. M. de Almeida, *Biosensors*, 2021, **11**, 82.

© 2024 The Author(s). Published by the Royal Society of Chemistry

Open Access Article. Published on 17 April 2024. Downloaded on 2/17/2026 1:49:50 PM.
This article is licensed under a Creative Commons Attribution 3.0 Unported Licence.

15 H. Ahangari, S. Kurbanoglu, A. Ehsani and B. Uslu, *Trends Food Sci. Technol.*, 2021, **112**, 75–87.
16 D. Sriramulu and S. Valiyaveettil, *Dyes Pigm.*, 2016, **134**, 306–314.
17 S. Ali, M. A. Jameel, G. Oldham, A. Gupta, M. Shafiei and S. J. Langford, *J. Mater. Chem. C*, 2022, **10**, 1326–1333.
18 Q. Deng, E. Zhou, Y. Huang, W. Qing, H. Zhai, Z. Liu and Z. Wei, *Chem. Commun.*, 2019, **55**, 4379–4382.
19 R. Roy, N. R. Sajeev, V. Sharma and A. L. Koner, *ACS Appl. Mater. Interfaces*, 2019, **11**, 47207–47217.
20 Y. Huang, S. Zhang, G. Zhong, C. Li, Z. Liu and D. Jin, *Phys. Chem. Chem. Phys.*, 2018, **20**, 19037–19044.
21 S. Ali, A. Gupta, M. Shafiei and S. J. Langford, *Chemosensors*, 2021, **9**, 30.
22 S. Chen, Z. Xue, N. Gao, X. Yang and L. Zang, *Sensors*, 2020, **20**, 917.
23 C. R. Harding, J. Cann, A. Laventure, M. Sadeghianlemraski, M. Abd-Ellah, K. R. Rao, B. S. Gelfand, H. Aziz, L. Kaake, C. Risko and G. C. Welch, *Mater. Horiz.*, 2020, **7**, 2959–2969.
24 E. Kozma and M. Catellani, *Dyes Pigm.*, 2013, **98**, 160–179.
25 P. Cheng, X. Zhao and X. Zhan, *Acc. Mater. Res.*, 2022, **3**, 309–318.
26 M. Courté, A. Hoff, G. C. Welch and L. G. Kaake, *J. Mater. Chem. C*, 2024, **12**, 5083–5087.
27 J. D. B. Koenig, W. E. Piers and G. C. Welch, *Chem. Sci.*, 2021, **13**, 1049–1059.
28 J. Cann, B. S. Gelfand and G. C. Welch, *Mol. Syst. Des. Eng.*, 2020, **5**, 1181–1185.
29 S. Mahajan and S. Jagtap, *Appl. Mater. Today*, 2020, **18**, 100483.
30 A. Kumar, G. Gupta, K. Bapna and D. D. Shivagan, *Mater. Res. Bull.*, 2023, **158**, 112053.
31 H.-E. Lin, Y. Katayanagi, T. Kishi, T. Yano and N. Matsushita, *RSC Adv.*, 2018, **8**, 30310–30319.
32 M. Parthibavarman, V. Hariharan and C. Sekar, *Mater. Sci. Eng., C*, 2011, **31**, 840–844.

© 2024 The Author(s). Published by the Royal Society of Chemistry